

## PROPAGATION OF COSMIC-RAY NUCLEONS IN THE GALAXY

ANDREW W. STRONG<sup>1</sup> AND IGOR V. MOSKALENKO<sup>1,2</sup>

<sup>1</sup>Max-Planck-Institut für extraterrestrische Physik, Postfach 1603, D-85740 Garching, Germany

<sup>2</sup>Institute for Nuclear Physics, M.V.Lomonosov Moscow State University, 119 899 Moscow, Russia

To appear in The Astrophysical Journal, 509:##-##, 1998 December 10

### ABSTRACT

We describe a method for the numerical computation of the propagation of primary and secondary nucleons, primary electrons, and secondary positrons and electrons. Fragmentation and energy losses are computed using realistic distributions for the interstellar gas and radiation fields, and diffusive reacceleration is also incorporated. The models are adjusted to agree with the observed cosmic-ray  $B/C$  and  $^{10}\text{Be}/^9\text{Be}$  ratios. Models with diffusion and convection do not account well for the observed energy dependence of  $B/C$ , while models with reacceleration reproduce this easily. The height of the halo propagation region is determined, using recent  $^{10}\text{Be}/^9\text{Be}$  measurements, as  $> 4$  kpc for diffusion/convection models and  $4 - 12$  kpc for reacceleration models. For convection models we set an upper limit on the velocity gradient of  $dV/dz < 7 \text{ km s}^{-1} \text{ kpc}^{-1}$ . The radial distribution of cosmic-ray sources required is broader than current estimates of the SNR distribution for all halo sizes. Full details of the numerical method used to solve the cosmic-ray propagation equation are given.

*Subject headings:* cosmic rays — diffusion — elementary particles — Galaxy: general — ISM: abundances — ISM: general

### 1. INTRODUCTION

A numerical method and corresponding computer code for the calculation of Galactic cosmic-ray propagation has been developed, which is a further development of the approach described by Strong & Youssefi (1995) and Strong (1996). Primary and secondary nucleons, primary and secondary electrons, and secondary positrons are included. The basic spatial propagation mechanisms are (momentum-dependent) diffusion and convection, while in momentum space energy loss and diffusive reacceleration are treated. Fragmentation and energy losses are computed using realistic distributions for the interstellar gas and radiation fields. Preliminary results were presented in Strong & Moskalenko (1997) (hereafter Paper I) and full results for protons, Helium, positrons, and electrons in Moskalenko & Strong (1998a) (hereafter Paper II). In Paper II we referred the description of the numerical method to the present paper (Paper III), and full details are now given. Results for gamma-rays and synchrotron radiation will be given in Moskalenko & Strong (1998b) (hereafter Paper IV).

We note that our positron predictions from Paper II have been compared with more recent absolute measurements in Barwick et al. (1998) and the agreement is good; for the positrons this new comparison has the advantage of being independent of the electron spectrum, unlike the positron/electron ratio which was the main focus of Paper II. The ultimate goal is to combine all constraints including gamma-ray and synchrotron spectra; this will be pursued in Paper IV.

The rationale for our approach was given previously (Paper I, Paper II). Briefly, the idea is to develop a model which simultaneously reproduces observational data of many kinds related to cosmic-ray origin and propagation: directly via measurements of nuclei, electrons, and positrons, indirectly via gamma rays and synchrotron radiation. These data provide many independent constraints on any model and our approach is able to take advantage of this since it must be consistent with all types of observation. We emphasize also the use of realistic astrophysical input (e.g. for the gas distribution) as well as the-

oretical developments (e.g. reacceleration). The code is sufficiently general that new physical effects can be introduced as required. We aim for a ‘standard model’ which can be improved with new astrophysical input and additional observational constraints. For interested users our model is available in the public domain on the World Wide Web.

It was pointed out many years ago (see Ginzburg, Khazan & Ptuskin 1980, Berezhinskii et al. 1990) that the interpretation of radioactive cosmic-ray nuclei is model-dependent and in particular that halo models lead to a quite different physical picture from homogeneous models. The latter show simply a rather lower average matter density than the local Galactic hydrogen (e.g., Simpson & Garcia-Munoz 1988, Lukasiak et al. 1994a), but do not lead to a meaningful estimate of the size of the confinement region, and the corresponding cosmic-ray ‘lifetime’ is model-dependent. In such treatments the lifetime is combined with the grammage to yield an ‘average density’. For example Lukasiak et al. (1994a) find an ‘average density’ of  $0.28 \text{ cm}^{-3}$  compared to the local interstellar value of about  $1 \text{ cm}^{-3}$ , indicating a  $z$ -extent of less than 1 kpc compared to the several kpc found in diffusive halo models. In the present work we use a model which includes spatial dimensions as a basic element, and so these issues are automatically addressed.

The possible rôle of convection was shown by Jokipii (1976), and Jones (1979) pointed out its effect on the energy-dependence of the secondary/primary ratio. Recent papers give estimates for the halo size and limits on convection based on existing calculations (e.g., Webber, Lee & Gupta 1992), and in the present work we attempt to improve on these models with a more detailed treatment.

Previous approaches to the spatial nucleon propagation problem have been mainly analytical: Jones (1979), Freedman et al. (1980), Berezhinskii et al. (1990), Webber, Lee & Gupta (1992) and Bloemen et al. (1993) treated diffusion/convection models in this way. A problem here is that energy losses are difficult to treat and in fact were apparently not included except by Webber, Lee & Gupta (1992), however even there not

explicitly. Bloemen et al. (1993) used the ‘grammage’ formulation rather than the explicit isotope ratios, and their propagation equation implicitly assumes identical distributions of primary and secondary source functions. These papers did not attempt to fit the low-energy ( $< 1$  GeV/nucleon)  $B/C$  data (which we will show leads to problems) and also did not consider reacceleration. It is clear that an analytical treatment quickly becomes limited as soon as more realistic models are desired, and this is the main justification for the numerical approach presented in this paper. The case of electrons and positrons is even more intractable analytically, although fairly general cases have been treated (Lerche & Schlickeiser 1982). Owens & Jokipii (1977a,b) adopted an alternative approach with Monte-Carlo simulations, for both nucleons and electrons. Recently Porter & Protheroe (1997) made use of this method for electrons. Both these applications are for 1-D propagation, in the  $z$ -direction only. This method allows realistic models to be computed, but would be very time-consuming for 2- or 3-D cases. Our method, using numerical solution of the propagation equation, is a practical alternative. Since most of these studies were done, the data on both stable and radioactive nuclei has improved considerably and thus a re-evaluation is warranted.

Reacceleration has previously been handled using leaky-box calculations (Letaw, Silberberg & Tsao 1993, Seo & Ptuskin 1994, Heinbach & Simon 1995); this has the advantage of allowing a full reaction network to be used (far beyond what is possible in the present approach), but suffers from the usual limitations of leaky-box models, especially concerning radioactive nuclei, which were not included in these treatments. Our simplified reaction network is necessary because of the added spatial dimensions, but we believe it is fully sufficient for our purpose, since we are not attempting to derive a comprehensive isotopic composition. A similar approach was followed by Webber, Lee & Gupta (1992). A more complex reaction scheme would not in any way change our conclusions.

We model convection in a simple way, taking a linear increase of velocity with  $z$ . Detailed self-consistent models of cosmic-ray driven MHD winds (Zirakashvili et al. 1996, Ptuskin et al. 1997) provide explicit predictions for the convective transport of cosmic-rays, and our approach could be used in future to evaluate the observational consequences of such models.

In this paper we concentrate on the evaluation of the  $B/C$  and  $^{10}\text{Be}/^9\text{Be}$  ratios, evaluation of diffusion/convection and reacceleration models, and on setting limits on the halo size. The  $B/C$  data is used since it is the most accurately measured ratio covering a wide energy range and having well established cross sections. The  $^{10}\text{Be}/^9\text{Be}$  ratio is used rather than  $^{10}\text{Be}/(^7\text{Be} + ^9\text{Be})$  since it is less sensitive to solar modulation and to rigidity effects in the propagation. A re-evaluation of the halo size is desirable since new  $^{10}\text{Be}/^9\text{Be}$  data are now available from Ulysses (Connell 1998) with better statistics than previously. It is not the purpose of this approach to perform detailed source abundance calculations with a large network of reactions, which is still best done with the path-length distribution approach (DuVernois, Simpson & Thayer 1996 and references therein). Instead we use just the principal progenitors and weighted cross sections based on the observed cosmic-ray abundances (see Webber, Lee & Gupta 1992). Other key cosmic-ray ratios such as  $^{26}\text{Al}/^{27}\text{Al}$  and sub- $Fe/Fe$  are beyond the scope of this paper but will be addressed in future work.

Also important are cosmic-ray gradients as derived from gamma rays; this provides a consistency check on the distribution of cosmic-ray sources, and we address this here.

## 2. DESCRIPTION OF THE MODELS

The models are three dimensional with cylindrical symmetry in the Galaxy, and the basic coordinates are  $(R, z, p)$ , where  $R$  is Galactocentric radius,  $z$  is the distance from the Galactic plane, and  $p$  is the total particle momentum. The distance from the Sun to the Galactic centre is taken as 8.5 kpc. In the models the propagation region is bounded by  $R = R_h$ ,  $z = z_h$  beyond which free escape is assumed. We take  $R_h = 30$  kpc. The range  $z_h = 1 - 20$  kpc is considered since this is suggested by previous studies of radioactive nuclei (e.g., Lukasiak et al. 1994a) and the distribution of synchrotron radiation (Phillipps et al. 1981). For a given  $z_h$  the diffusion coefficient as a function of momentum is determined by  $B/C$  for the case of no reacceleration; if reacceleration is assumed then the reacceleration strength (related to the Alfvén speed) is constrained by the energy-dependence of  $B/C$ . The spatial diffusion coefficient for the case of no reacceleration is taken as  $D_{xx} = \beta D_0(\rho/\rho_0)^{\delta_1}$  below rigidity  $\rho_0$ ,  $\beta D_0(\rho/\rho_0)^{\delta_2}$  above rigidity  $\rho_0$ , where the factor  $\beta (= v/c)$  is a natural consequence of a random-walk process. Since the introduction of a sharp break in  $D_{xx}$  is an extremely contrived procedure which is adopted just to fit  $B/C$  at all energies, we also consider the case  $\delta_1 = \delta_2$ , i.e. no break, in order to investigate the possibility of reproducing the data in a physically simpler way<sup>1</sup>. The convection velocity (in  $z$ -direction only)  $V(z)$  is assumed to increase linearly with distance from the plane ( $V > 0$  for  $z > 0$ ,  $V < 0$  for  $z < 0$ , and  $dV/dz > 0$  for all  $z$ ). This implies a constant adiabatic energy loss; the possibility of adiabatic energy gain ( $dV/dz < 0$ ) is not considered. The linear form for  $V(z)$  is consistent with cosmic-ray driven MHD wind models (e.g., Zirakashvili et al. 1996). The velocity at  $z = 0$  is a model parameter, but we consider here only  $V(0) = 0$ .

Some stochastic reacceleration is inevitable, and it provides a natural mechanism to reproduce the energy dependence of the  $B/C$  ratio without an *ad hoc* form for the diffusion coefficient (Letaw, Silberberg & Tsao 1993, Seo & Ptuskin 1994, Heinbach & Simon 1995, Simon & Heinbach 1996). The spatial diffusion coefficient for the case of reacceleration assumes a Kolmogorov spectrum of weak MHD turbulence so  $D_{xx} = \beta D_0(\rho/\rho_0)^\delta$  with  $\delta = 1/3$  for all rigidities. Simon and Heinbach (1995) showed that the Kolmogorov form best reproduces the observed  $B/C$  variation with energy. For the case of reacceleration the momentum-space diffusion coefficient  $D_{pp}$  is related to the spatial coefficient using the formula given by Seo & Ptuskin (1994) (their equation [9]), and Berezhinskii et al. (1990)

$$D_{pp}D_{xx} = \frac{4p^2 v_A^2}{3\delta(4-\delta^2)(4-\delta)w}, \quad (1)$$

where  $w$  characterises the level of turbulence, and is equal to the ratio of MHD wave energy density to magnetic field energy density. The main free parameter in this relation is the Alfvén speed  $v_A$ ; we take  $w = 1$  (Seo & Ptuskin 1994) but clearly only the quantity  $v_A^2/w$  is relevant.

The atomic hydrogen distribution is represented by the formula

$$n_{HI}(R, z) = n_{HI}(R) e^{-\ln^2(z/z_0)^2}, \quad (2)$$

where  $n_{HI}(R)$  is taken from Gordon & Burton (1976) and  $z_0$

<sup>1</sup>In Paper II we considered only  $\delta_1 = 0$  and did not consider convection

from Cox, Krügel & Mezger (1986) giving an exponential increase in the width of the  $HI$  layer outside the solar circle:

$$z_0(R) = \begin{cases} 0.25 \text{ kpc}, & R \leq 10 \text{ kpc}; \\ 0.083 e^{0.11R} \text{ kpc}, & R > 10 \text{ kpc}. \end{cases} \quad (3)$$

The distribution of molecular hydrogen is taken from Bronfman et al. (1988) using  $CO$  surveys:

$$n_{H_2}(R, z) = n_{H_2}(R) e^{-\ln 2 \cdot (z/70 \text{ pc})^2}. \quad (4)$$

The adopted radial distribution of  $HI$  and  $H_2$  is shown in Figure 1.

For the ionized gas we use the two-component model of Cordes et al. (1991):

$$n_{HII} = 0.025 e^{-\frac{|z|}{1 \text{ kpc}} - \left(\frac{R}{20 \text{ kpc}}\right)^2} + 0.2 e^{-\frac{|z|}{0.15 \text{ kpc}} - \left(\frac{R}{2 \text{ kpc}} - 2\right)^2} \text{ cm}^{-3}. \quad (5)$$

The first term represents the extensive warm ionized gas and is similar to the distribution given by Reynolds (1989); the second term represents  $HII$  regions and is concentrated around  $R = 4$  kpc. A temperature of  $10^4$  K is assumed to compute Coulomb energy losses in ionized gas.

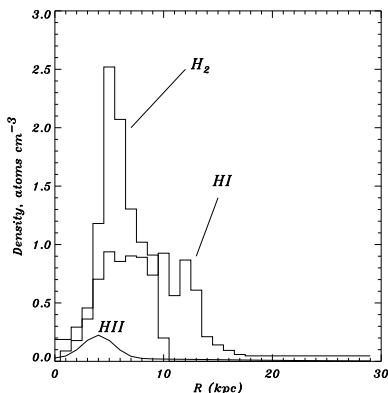


FIG. 1.— The adopted radial distribution of atomic, molecular and ionized hydrogen at  $z = 0$ .

The  $He/H$  ratio of the interstellar gas is taken as 0.11 by number; there is some uncertainty in this quantity, but our value is consistent with recent photospheric determinations ( $0.10 \pm 0.008$ : Grevesse, Noels & Sauval 1996). Helioseismological methods (Hernandez & Christensen-Dalsgaard 1994) give a Helium abundance by mass of 0.242 corresponding to  $He/H = 0.08$ , but still with possible uncertainties due to the details of the models. Although the latter is perhaps the most accurate local determination, the uncertainty in extending the photospheric value to the interstellar medium over the whole Galaxy is large. Other uncertainties dominate the secondary production, for example the density of neutral and molecular hydrogen. In any case, even if  $He/H = 0.08$  the influence of the uncertainty of  $He/H$  on the secondary production does not exceed 10%.

The distribution of cosmic-ray sources is chosen to reproduce (after propagation) the cosmic-ray distribution determined by analysis of EGRET gamma-ray data (Strong & Mattox 1996). The form used is

$$q(R, z) = q_0 \left( \frac{R}{R_\odot} \right)^\eta e^{-\xi \frac{R-R_\odot}{R_\odot} - \frac{|z|}{0.2 \text{ kpc}}}, \quad (6)$$

where  $q_0$  is a normalization constant,  $\eta$  and  $\xi$  are parameters; the  $R$ -dependence has the same parameterization as that used for SNR by Case & Bhattacharya (1996), but we adopt different parameters in order to fit the gamma-ray gradient. We also compute models with the SNR distribution, to investigate the possibility of fitting the gradient in this case. We apply a cut-off in the source distribution at  $R = 20$  kpc since it is unlikely that significant sources are present at such large radii. The  $z$ -dependence of  $q$  is nominal and reflects simply the assumed confinement of sources to the disk.

We assume that the source distribution of all cosmic-ray primaries is the same. Meyer, Drury & Ellison (1997) suggest that part of the C and O originates in acceleration of C and O enriched pre-SN Wolf-Rayet wind material by supernovae, but the source distribution in this case would still follow that of SNR.

The primary propagation is computed first giving the primary distribution as a function of  $(R, z, p)$ ; then the secondary source function is obtained from the gas density and cross sections, and finally the secondary propagation is computed. Tertiary reactions, such as  $^{11}B \rightarrow ^{10}B$  are treated as described in Appendix A. The entire calculation is performed with momentum as the kinematic variable, since this greatly facilitates the inclusion of reacceleration.

Full details of the propagation equation and numerical method used are given in Appendices A and B. The method encompasses nucleons, electrons and positrons. Energy losses for nucleons by ionization and Coulomb interactions are included following Mannheim & Schlickeiser (1994) (see Appendix C.1). Details of the positron source function, magnetic field and interstellar radiation field models were given in Paper II, and the energy loss formulae for electrons are given in the present paper in Appendix C.2.

As an illustration of the calculations performed by the code, Figure 2 shows the  $(R, z)$  distribution of primary  $^{12}C$  and secondary  $^{10,11}B$  at 515 MeV/nucleon for a reacceleration model with  $z_h = 10$  kpc. In practice we are only interested in the isotope ratios at the solar position, but it is worth noting the variations over the Galaxy, which are due to effect of the inhomogeneous distribution of sources and gas on the secondary production, fragmentation and energy losses. For comparison with gamma-ray data the full 3-D distribution is of course important and will be addressed in Paper IV, but here only the radial cosmic-ray gradient from gamma-rays is considered.

### 3. EVALUATION OF MODELS

We consider the cases of diffusion+convection and diffusion+reacceleration, since these are the minimum combinations which can reproduce the key observations. In principle all three processes could be significant, and such a general model can be considered if independent astrophysical information or models, for example for a Galactic wind (e.g., Zirakashvili et al. 1996, Ptuskin et al. 1997), were to be used. Anticipating the results, it can be noted at the outset that the reacceleration models are more satisfactory in meeting the constraints provided by the data, reproducing the  $B/C$  energy dependence without *ad hoc* variations in the diffusion coefficient; further it is not possible to find any *simple* version of the diffusion/convection model which reproduces  $B/C$  satisfactorily without additional special assumptions.

In our calculations we use the  $B/C$  data summarized by Webber et al. (1996), from HEAO-3 and Voyager 1 and 2. The spectra were modulated to 500 MV appropriate to this data using the

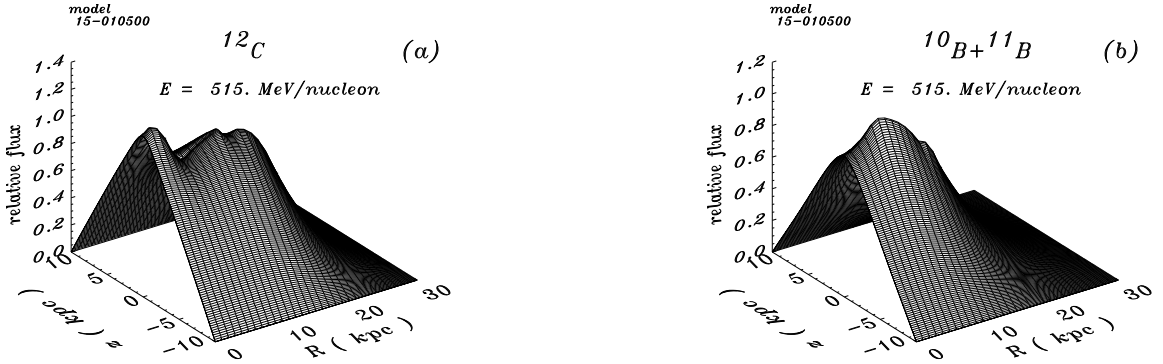


FIG. 2.— The 3-D distribution of  $^{12}\text{C}$  and  $^{10,11}\text{B}$  at 515 MeV/nucleon for reacceleration model with  $z_h = 10$  kpc, for  $v_A = 20$  km  $\text{s}^{-1}$ . Parameters: see model 10500 in Table 2.

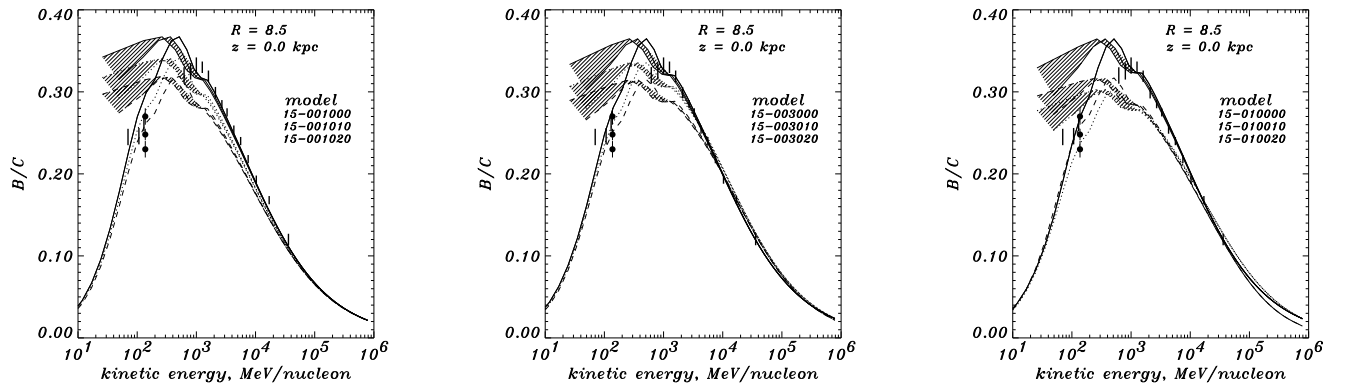


FIG. 3.—  $B/C$  ratio for diffusion/convection models without break in diffusion coefficient, for  $dV/dz = 0$  (solid lines), 5 (dotted lines), and 10  $\text{km s}^{-1} \text{kpc}^{-1}$  (dashed lines). The cases shown are (a)  $z_h = 1$  kpc, (b)  $z_h = 3$  kpc, (c)  $z_h = 10$  kpc. Solid lines: interstellar ratio, shaded area: modulated to 300 – 500 MV. Data: vertical bars: HEAO-3, Voyager (Webber et al. 1996), filled circles: Ulysses (DuVernois, Simpson & Thayer 1996:  $\Phi = 600, 840, 1080$  MV). Parameters as in Table 1.

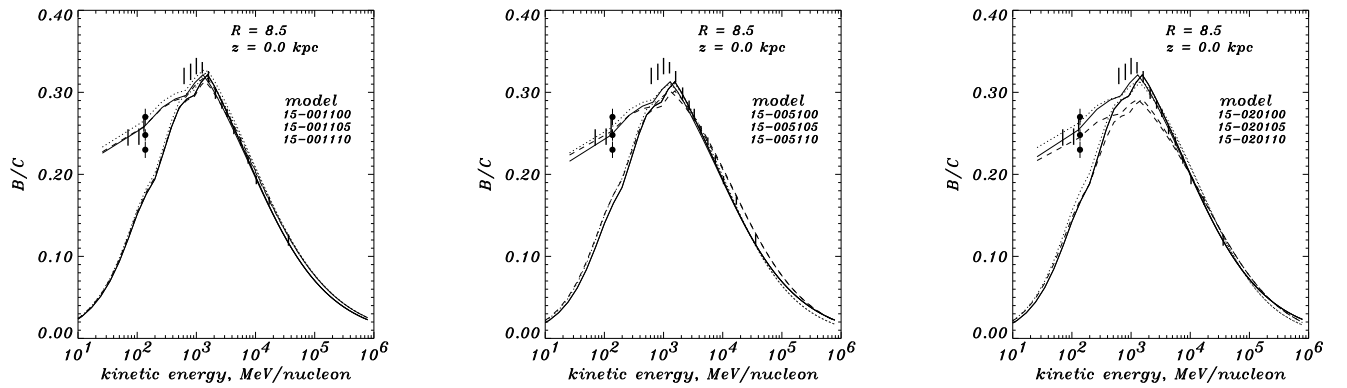


FIG. 4.—  $B/C$  ratio for diffusion/convection models with break in diffusion coefficient, for  $dV/dz = 0$  (solid lines), 5 (dotted lines), and 10  $\text{km s}^{-1} \text{kpc}^{-1}$  (dashed lines). The cases shown are (a)  $z_h = 1$  kpc, (b)  $z_h = 5$  kpc, (c)  $z_h = 20$  kpc. Lower lines: interstellar ratio; upper lines: modulated to 500 MV. Parameters as in Table 1. Data: as Figure 3.

force-field approximation (Gleeson & Axford 1968). We also show  $B/C$  values from Ulysses (DuVernois, Simpson & Thayer 1996) for comparison, but since this has large modulation (600 – 1080 MV) we do not base conclusions on these values. We use the measured  $^{10}\text{Be}/^9\text{Be}$  ratio from Ulysses (Connell 1998) and from Voyager-1,2, IMP-7/8, ISEE-3 as summarized by Lukasiak et al. (1994a).

The source distribution adopted has  $\eta = 0.5$ ,  $\xi = 1.0$  in eq. (6) (apart from the cases with SNR source distribution). This form adequately reproduces the small observed gamma-ray based gradient, for all  $z_h$ ; a more detailed discussion is given in Section 4.

### 3.1. Diffusion/convection models

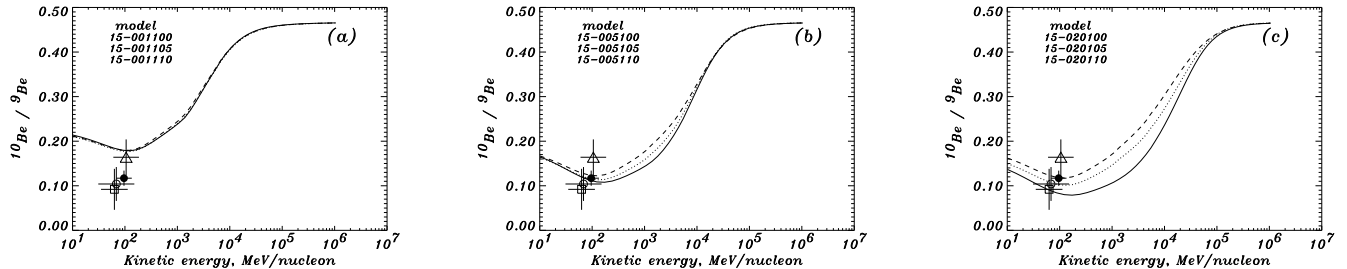


FIG. 5.—  $^{10}\text{Be}/^9\text{Be}$  ratio for diffusion/convection models, for  $dV/dz = 0$  (solid lines), 5 (dotted lines), and  $10 \text{ km s}^{-1} \text{ kpc}^{-1}$  (dashed lines). The cases shown are (a)  $z_h = 1 \text{ kpc}$ , (b)  $z_h = 5 \text{ kpc}$ , (c)  $z_h = 20 \text{ kpc}$ . Data points from Lukasiak et al. (1994a) (Voyager-1,2: square, IMP-7/8: open circle, ISEE-3: triangle) and Connell (1997) (Ulysses): filled circle. Parameters as in Table 1.

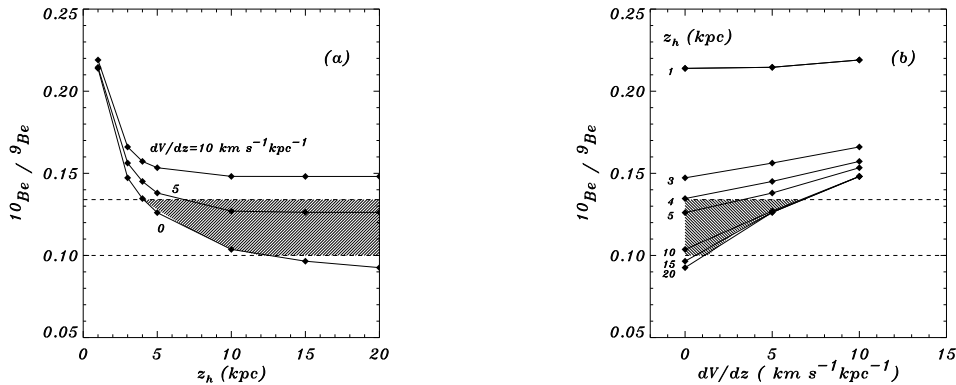


FIG. 6.— Predicted  $^{10}\text{Be}/^9\text{Be}$  ratio as function of (a)  $z_h$  for  $dV/dz = 0, 5, 10 \text{ km s}^{-1} \text{ kpc}^{-1}$ , (b)  $dV/dz$  for  $z_h = 1-20 \text{ kpc}$  at  $525 \text{ MeV/nucleon}$  corresponding to the mean interstellar value for the Ulysses data (Connell 1998); the Ulysses experimental limits are shown as horizontal dashed lines. The shaded regions show the parameter ranges allowed by the data.

The main parameters are  $z_h$ ,  $D_0$ ,  $\delta_1$ ,  $\delta_2$  and  $\rho_0$  and  $dV/dz$ . We treat  $z_h$  as the main unknown quantity, and consider values  $1 - 20 \text{ kpc}$ . The parameters of these models are summarized in Table 1. For a given  $z_h$  we show  $B/C$  for a series of models with different  $dV/dz$ .

Figure 3 shows the case of no break,  $\delta_1 = \delta_2$ ; for each  $dV/dz$ , the remaining parameters  $D_0$ ,  $\delta_1$  and  $\rho_0$  are adjusted to fit the data as well as possible. It is clear that a *good* fit is *not* possible; the basic effect of convection is to reduce the variation of  $B/C$  with energy, and although this improves the fit at low energies the characteristic peaked shape of the measured  $B/C$  cannot be reproduced. Although modulation makes the comparison with the low energy Voyager data somewhat uncertain, Figure 3 shows that the fit is unsatisfactory; the same is true even if we use a very low modulation parameter of  $300 \text{ MV}$  in an attempt to improve the fit. This modulation is near the minimum value for the entire Voyager 17 year period (cf. the average value of  $500 \text{ MV}$ ; Webber et al. 1996). The failure to obtain a good fit is an important conclusion since it shows that the simple inclusion of convection cannot solve the problem of the low-energy falloff in  $B/C$ .

Since the inclusion of a convective term is nevertheless of interest for independent astrophysical reasons (Galactic wind) we can force a fit to the data by allowing a break in  $D_{xx}(p)$ , with  $\delta_1 \neq \delta_2$ . Figure 4 shows cases with a break: here the parameters  $D_0$ ,  $\delta_1$ ,  $\delta_2$  and  $\rho_0$  are adjusted. In the absence of convection, the falloff in  $B/C$  at low energies requires that the diffusion coeffi-

cient increases rapidly below  $\rho_0 = 3 \text{ GV}$  ( $\delta_1 \sim -0.6$ ) reversing the trend from higher energies ( $\delta_2 \sim +0.6$ ). Inclusion of the convective term does not reduce the size of the *ad hoc* break in the diffusion coefficient, in fact it rather exacerbates the problem by requiring a larger break<sup>2</sup>.

Figure 5 shows the predicted and measured  $^{10}\text{Be}/^9\text{Be}$  ratio; here we use the models with a break in  $D_{xx}(p)$  since these do have the correct  $B/C$  ratio in the few  $100 \text{ MeV/nucleon}$  range where the  $\text{Be}$  measurements are available and are therefore appropriate for this comparison independently of the situation at higher energies. For our final evaluation we use  $^{10}\text{Be}/^9\text{Be}$  data from Ulysses, which has the highest statistics.

Figure 6 summarizes the limits on  $z_h$  and  $dV/dz$ , using the  $^{10}\text{Be}/^9\text{Be}$  ratio at the interstellar energy of  $525 \text{ MeV/nucleon}$  appropriate to the Ulysses data (Connell 1998). For  $z_h < 4 \text{ kpc}$ , the predicted ratio is always too high, even for no convection; no convection is allowed for such  $z_h$  values since this increases  $^{10}\text{Be}/^9\text{Be}$  still further. For  $z_h \geq 4 \text{ kpc}$  agreement with  $^{10}\text{Be}/^9\text{Be}$  is possible provided  $0 < dV/dz < 7 \text{ km s}^{-1} \text{ kpc}^{-1}$ . We conclude from Figure 6a that in the absence of convection  $4 \text{ kpc} < z_h < 12 \text{ kpc}$ , and if convection is allowed the lower limit remains but no upper limit can be set. It is interesting that an upper as well as a lower limit on  $z_h$  is obtained in the case of no convection, although  $^{10}\text{Be}/^9\text{Be}$  approaches asymptotically a constant value for large halo sizes and becomes insensitive to the halo dimension. From Figure 6b,  $dV/dz < 7$

<sup>2</sup>Note that the dependence of interaction rate on particle velocity itself is not sufficient to cause the full observed low-energy falloff. In leaky-box treatments the low-energy behaviour is modelled by adopting a constant path-length below a few  $\text{GeV/nucleon}$ , without attempting to justify this physically. A convective term is often invoked, but our treatment shows that this alone is not sufficient.

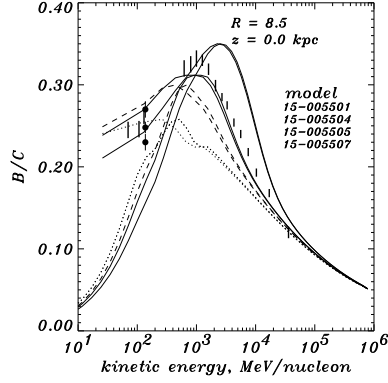


FIG. 7.—  $B/C$  ratio for diffusive reacceleration models with  $z_h = 5$  kpc,  $v_A = 0$  (dotted), 15 (dashed), 20 (thin solid), 30  $\text{km s}^{-1}$  (thick solid). Parameters as in Table 2. In each case the interstellar ratio and the ratio modulated to 500 MV is shown. Data: as Figure 3.

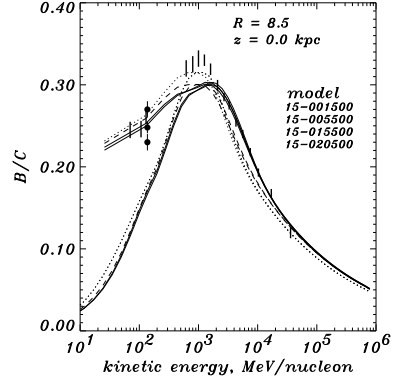


FIG. 8.—  $B/C$  ratio for diffusive reacceleration models:  $z_h = 1$  (dotted), 5 (dashed), 10 (thin solid), and 20 kpc (thick solid). Parameters as in Table 2. In each case the interstellar ratio and the ratio modulated to 500 MV is shown. Data: as Figure 3.

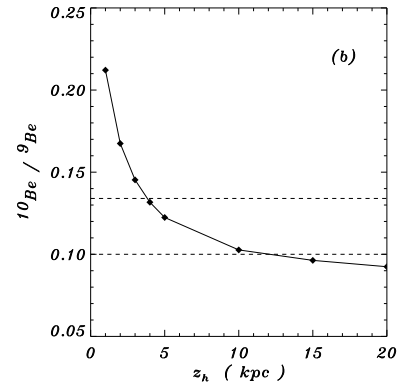
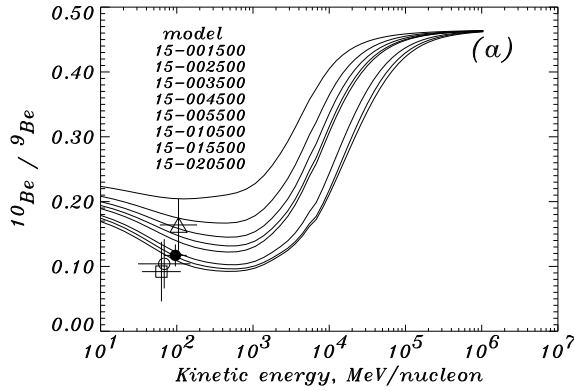


FIG. 9.—  $^{10}\text{Be}/^9\text{Be}$  ratio for diffusive reacceleration models: (a) as function of energy for (from top to bottom)  $z_h = 1, 2, 3, 4, 5, 10, 15$  and 20 kpc, data points as in Figure 5; (b) as function of  $z_h$  at 525 MeV/nucleon corresponding to the mean interstellar value for the Ulysses data (Connell 1998); the Ulysses experimental limits are shown as horizontal dashed lines. Parameters as in Table 2.

$\text{km s}^{-1} \text{ kpc}^{-1}$  and this figure places upper limits on the convection parameter for each halo size. These limits are rather strict, and a finite wind velocity is only allowed in any case for  $z_h > 4$  kpc. Note that these results are not very sensitive to modulation since the predicted  $^{10}\text{Be}/^9\text{Be}$  is fairly constant from 100 to 1000 MeV/nucleon.

Our results can be compared with those of other studies:  $z_h \geq 7.8$  kpc (Freedman et al. 1980),  $z_h \leq 3$  kpc (Bloemen et al. 1993), and  $z_h \leq 4$  kpc (Webber, Lee & Gupta 1992). Most recently Lukasiak et al. (1994a) found  $1.9 \text{ kpc} < z_h < 3.6 \text{ kpc}$  (for no convection) based on Voyager  $\text{Be}$  data and using the Webber, Lee & Gupta (1992) models. We believe our new limits to be an improvement, first because of the improved  $\text{Be}$  data from Ulysses, second because of our treatment of energy losses (see Section 3.2) and generally more realistic astrophysical details in our model. The papers cited also did not consider the low-energy  $B/C$  data, which we have shown are in fact a problem for diffusion/convection models.

The cosmic-ray driven wind models of Zirakashvili et al. (1996) have values of  $dV/dz \approx 10 \text{ km s}^{-1} \text{ kpc}^{-1}$ , somewhat larger than our upper limits. Since their models are different from ours in many respects this is not significant, but suggests it would be useful to carry out calculations like those in the present paper for such models to provide a critical test of their

viability.

### 3.2. Diffusive reacceleration models

The main parameters are  $z_h$ ,  $D_0$  and  $v_A$  ( $\rho_0$  is arbitrary since  $\delta$  is constant). Again we treat  $z_h$  as the main unknown quantity. The evaluation is simpler than for convection models since the number of free parameters is smaller. The parameters of these models are summarized in Table 2. Figure 7 illustrates the effect on  $B/C$  of varying  $v_A$ , from  $v_A = 0$  (no reacceleration) to  $v_A = 30 \text{ km s}^{-1}$ , for  $z_h = 5$  kpc. This shows how the initial form becomes modified to produce the characteristic peaked shape. Reacceleration models thus lead naturally to the observed peaked form of  $B/C$ , as pointed out by several previous authors (e.g., Letaw, Silberberg & Tsao 1993, Seo & Ptuskin 1994, Heinbach & Simon 1995).

Figure 8 shows  $B/C$  for  $z_h = 1 - 20$  kpc. Our value of  $v_A \approx 20 \text{ km s}^{-1}$  is consistent with the value obtained by Seo & Ptuskin (1994) which they also derived from  $B/C$ ; since for stable nuclei the leaky-box and diffusion treatments are equivalent this is a good test of the operation of our code. The value of  $v_A$  is typical of the warm ionized phase of the interstellar gas (Seo & Ptuskin 1994). The exact low-energy form of  $B/C$  depends on details of the modulation so that an exact fit here is not attempted; note however that  $v_A$  and  $D_0$  can be (and indeed

TABLE 1  
PARAMETERS OF DIFFUSION/CONVECTION MODELS.

Model	$z_h$ kpc	$D_0$ $10^{28} \text{ cm}^2 \text{ s}^{-1}$	$\rho_0$ GV	$\delta_1$	$\delta_2$	$dV/dz$ $\text{km s}^{-1} \text{ kpc}^{-1}$
01000	1	0.7	3	0.60	0.60	0
01010	1	0.7	3	0.60	0.60	10
01020	1	0.7	3	0.60	0.60	20
03000	3	2.0	3	0.60	0.60	0
03010	3	1.4	3	0.65	0.65	10
03020	3	1.1	3	0.70	0.70	20
10000	10	5.0	3	0.60	0.60	0
10010	10	2.5	3	0.70	0.70	10
10020	10	1.1	3	0.90	0.90	20
01100	1	0.9	5	-0.60	0.60	0
01105	1	0.8	5	-0.60	0.60	5
01110	1	0.8	5	-0.60	0.60	10
03100	3	2.5	5	-0.60	0.60	0
03105	3	2.2	5	-0.60	0.60	5
03110	3	2.0	5	-0.60	0.60	10
04100	4	3.5	5	-0.60	0.60	0
04105	4	2.7	5	-0.60	0.70	5
04110	4	2.5	5	-0.60	0.70	10
05100	5	4.5	5	-0.60	0.60	0
05105	5	3.2	5	-0.60	0.70	5
05110	5	2.5	5	-0.60	0.70	10
10100	10	7.0	5	-0.60	0.60	0
10105	10	3.8	5	-0.60	0.80	5
10110	10	3.0	5	-0.60	0.80	10
15100	15	9.0	5	-0.60	0.60	0
15105	15	3.8	5	-0.60	0.80	5
15110	15	3.0	5	-0.60	0.80	10
20100	20	9.0	5	-0.60	0.60	0
20105	20	3.8	5	-0.60	0.80	5
20110	20	3.0	5	-0.60	0.80	10

TABLE 2  
PARAMETERS OF DIFFUSIVE REACCELERATION MODELS<sup>a</sup>

Best fit models <sup>b</sup>	Models with no energy losses <sup>b</sup>	Models with SNR source distribution <sup>c</sup>	$z_h$ kpc	$D_0$ $10^{28} \text{ cm}^2 \text{ s}^{-1}$	$v_A$ $\text{km s}^{-1}$
01500	01510	01511	1	1.7	20
02500	02510	02511	2	3.2	20
03500	03510	03511	3	4.6	20
04500	04510	04511	4	6.0	20
05500	05510	05511	5	7.7	20
10500	10510	10511	10	12	20
15500	15510	15511	15	15	20
20500	20510	20511	20	16	18
Effect of varying $v_A$ :					
05501	...	...	5	7.7	0
05502	...	...	5	7.7	5
05503	...	...	5	7.7	10
05504	...	...	5	7.7	15
05505	...	...	5	7.7	20
05506	...	...	5	7.7	25
05507	...	...	5	7.7	30

<sup>a</sup>For all reacceleration models  $\rho_0 = 3 \text{ GV}$ ,  $\delta = 1/3$  (see Section 2 for details)

<sup>b</sup>Parameters of the source distribution (eq. [6]):  $\eta = 0.5, \xi = 1.0$

<sup>c</sup>Parameters of the SNR distribution (eq. [6]):  $\eta = 1.69, \xi = 3.33$

were) determined from the high-energy  $B/C$  alone, and the low-energy agreement is then satisfactory<sup>3</sup>. Figure 9 shows  $^{10}\text{Be}/^9\text{Be}$  for the same models, (a) as a function of energy for various  $z_h$ , (b) as a function of  $z_h$  at 525 MeV/nucleon corresponding to the Ulysses measurement. Comparing with the Ulysses data point, we conclude that  $4 \text{ kpc} < z_h < 12 \text{ kpc}$ . Again the result is not very sensitive to modulation since the predicted  $^{10}\text{Be}/^9\text{Be}$  is fairly constant from 100 to 1000 MeV/nucleon.

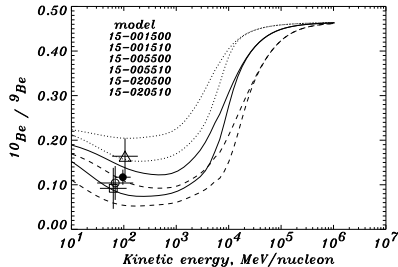


FIG. 10.—  $^{10}\text{Be}/^9\text{Be}$  ratio for diffusive reacceleration model, showing influence of energy losses, for  $z_h = 1 \text{ kpc}$  (dotted lines),  $5 \text{ kpc}$  (solid),  $20 \text{ kpc}$  (dashed). In each case upper curve is with energy losses, lower curve without. Parameters as in Table 2. Data points as in Figure 5.

Figure 10 illustrates the importance of energy losses on the  $^{10}\text{Be}/^9\text{Be}$  ratio; for reacceleration cases with  $z_h = 1 - 20 \text{ kpc}$ , we show the ratio with and without losses. Losses attenuate the flux of stable nuclei much more than radioactive nuclei, and hence lead to an increase in  $^{10}\text{Be}/^9\text{Be}$ . The effect can be simply illustrated as follows. The ionization loss rate on neutral gas is  $\sim 1.8 \times 10^{-7} Z^2 \langle n_H \rangle \beta^{-1} \text{ eV s}^{-1}$ , where  $\beta = v/c$  is the nucleon speed, and  $\langle n_H \rangle$  is the average interstellar gas density. Thus for  $\text{Be}$ -nuclei of  $300 \text{ MeV/nucleon}$  and for a gas disk with  $0.2 \text{ kpc}$  thickness and density  $1 \text{ cm}^{-3}$ ,  $\langle n_H \rangle = 0.2/z_h \text{ cm}^{-3}$ , which gives the loss time of  $\sim 3 \times 10^8$  years for  $z_h = 5 \text{ kpc}$ . Coulomb losses on the ionized gas in the halo increase the losses further (see Figure 13); although the density is low the wide  $z$ -extent means that the losses occur over large regions of the halo. For the same  $z_h$  the diffusion time is  $\approx 4 \times 10^8$  years so the stable  $^9\text{Be}$  is significantly attenuated. For the radioactive  $^{10}\text{Be}$  ( $\tau_{1/2} = 1.6 \times 10^6$  years) the energy losses are negligible. Hence losses significantly increase  $^{10}\text{Be}/^9\text{Be}$ . As can be seen in Figure 10, the relative effect is largest for large halos and becomes a dominant effect only for  $z_h > 3 \text{ kpc}$ . Although we illustrate this for the reacceleration case, the same effect applies to diffusion/convection models. Clearly if losses are ignored the predicted ratio will be too low and the derived value of  $z_h$  will be too small since  $z_h$  will have to be reduced to fit the observations.

The proton, Helium and positron spectra were presented in Paper II for the case  $z_h = 3 \text{ kpc}$  using the same model as used here, and the injection spectra were derived. The effect of varying the halo size is small for these spectra so we do not extend that calculation to different  $z_h$ .

#### 4. COSMIC-RAY GRADIENTS

An important constraint on any model of cosmic-ray propagation is provided by gamma-ray data which give information on the radial distribution of cosmic rays in the Galaxy. For a given source distribution, a large halo will give a smaller cosmic-ray gradient. It is generally believed that supernova remnants (SNR) are the main sources of cosmic rays (see Web-

ber 1997 for a recent review), but unfortunately the distribution of SNR is poorly known due to selection effects. Nevertheless it is interesting to compare quantitatively the effects of halo size on the gradient for a plausible SNR source distribution. For illustration we use the SNR distribution from Case & Bhattacharya (1996), which is peaked at  $R = 4 - 5 \text{ kpc}$  and has a steep falloff towards larger  $R$ .

Figure 11 shows the effect of halo size on the resulting radial distribution of  $3 \text{ GeV}$  cosmic-ray protons, for the reacceleration model. For comparison we show the cosmic-ray distribution deduced by model-fitting to EGRET gamma-ray data ( $> 100 \text{ MeV}$ ) from Strong & Mattox (1996), which is dominated by the  $\pi^0$ -decay component generated by  $\text{GeV}$  nucleons; the analysis by Hunter et al. (1997), based on a different approach, gives a similar result. The predicted cosmic-ray distribution using the SNR source function is too steep even for large halo sizes; in fact the halo size has a relatively small effect on the distribution. Other related distributions such as pulsars (Taylor, Manchester & Lyne 1993, Johnston 1994) have an even steeper falloff. Only for  $z_h = 20 \text{ kpc}$  does the gradient approach that observed, and in this case the combination of a large halo and a slightly less steep SNR distribution could give a satisfactory fit. For diffusion/convection models the situation is similar, with more convection tending to make the gradient follow more closely the sources. A larger halo ( $z_h \gg 20 \text{ kpc}$ ), apart from being excluded by the  $^{10}\text{Be}$  analysis presented here, would in fact not improve the situation much since Fig. 11 shows that the gradient approaches an asymptotic shape which hardly changes beyond a certain halo size. This is a consequence of the nature of the diffusive process, which even for an unlimited propagation region still retains the signature of the source distribution.

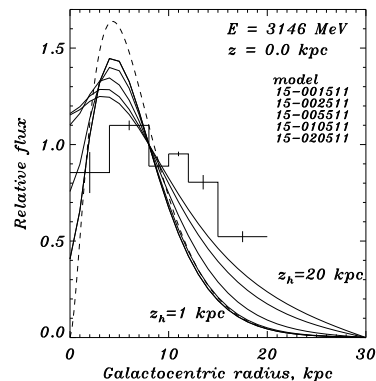


FIG. 11.— Radial distribution of  $3 \text{ GeV}$  protons at  $z = 0$ , for diffusive reacceleration model with halo sizes  $z_h = 1, 3, 5, 10, 15,$  and  $20 \text{ kpc}$  (solid curves). The source distribution is that for SNR given by Case & Bhattacharya (1996), shown as a dashed line. The cosmic-ray distribution deduced from EGRET  $> 100 \text{ MeV}$  gamma rays (Strong & Mattox 1996) is shown as the histogram. Parameters as in Table 2.

Based on these results we have to conclude, in the context of the present models, that the distribution of sources is not that expected from the (highly uncertain: see Green 1991) distribution of SNR. This conclusion is similar to that previously found by others (Webber, Lee & Gupta 1992, Bloemen et al. 1993). In view of the difficulty of deriving the SNR distribution this is perhaps not a serious shortcoming; if SNR are indeed CR sources then it is possible that the gamma-ray analysis gives the best estimate of their Galactic distribution. Therefore in our

<sup>3</sup>Since we are considering a *ratio* at the same rigidity the effect of modulation is confined to a deceleration  $\approx 200 \text{ MeV/nucleon}$  (cf. spectra where absolute intensity changes are important).



standard model we have obtained the source distribution empirically by requiring consistency with the high-energy gamma-ray results.

Figure 12 shows the source distribution adopted in the present work, and the resulting 3 GeV proton distribution, again compared to that deduced from gamma rays. The gradients are now consistent, especially considering that some systematic effects, due for example unresolved gamma-ray sources, are present in the gamma-ray results.

Measurements of cosmic-ray anisotropy in the 1 – 100 TeV range provide an independent argument for reacceleration (e.g., Seo & Ptuskin 1994) since the slower increase of diffusion coefficient with energy avoids the large anisotropies predicted by non-reacceleration models. Our models reproduce this behaviour, the reacceleration models giving anisotropies  $\sim 10^{-3}$  at 1 TeV, while the non-reacceleration models give  $> 10^{-2}$ . The observed values ( $\sim 10^{-3}$ ) largely reflect the local structure of the interstellar magnetic field in the part of the Galaxy near the Sun, and hence do not give useful constraints on the large-scale propagation which our model addresses (see Berezhinskii et al. 1990). In particular it is not possible to test the large-scale cosmic-ray gradients at such energies by this method. It is sufficient to note that the reacceleration models are consistent with the observations while the non-reacceleration models are not, in accord with previous authors' conclusions.

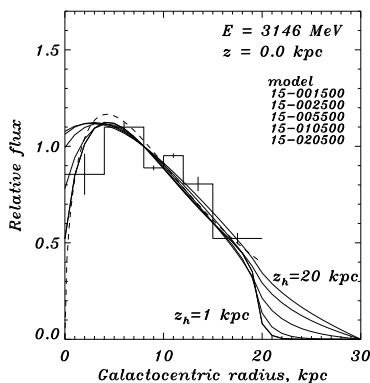


FIG. 12.— Radial distribution of 3 GeV protons at  $z = 0$ , for diffusive reacceleration model with various halo sizes  $z_h = 1, 3, 5, 10, 15$ , and 20 kpc (solid curves). The source distribution used is shown as a dashed line, and is that adopted to reproduce the cosmic-ray distribution deduced from EGRET  $> 100$  MeV gamma rays (Strong & Mattox 1996), shown as the histogram. Parameters as in Table 2.

## 5. CONCLUSIONS

We have shown that simple diffusion/convection models have difficulty in accounting for the observed form of the  $B/C$  ratio without special assumptions chosen to fit the data, and do not obviate the need for an *ad hoc* form for the diffusion coefficient. On the other hand we confirm the conclusion of other authors that models with reacceleration account naturally for the energy dependence over the whole observed range, with only two free parameters. Combining these results points rather strongly in favour of the reacceleration picture. In this case  $v_A \approx 20$  km  $s^{-1}$ , with little dependence on  $z_h$ .

For the first time  $^{10}Be/^{9}Be$  has also been computed with reacceleration. We take advantage of the recent Ulysses  $Be$  measurements to improve limits on the halo size. We emphasize the crucial importance of the treatment of energy losses in the evaluation of the  $^{10}Be/^{9}Be$  ratio. The halo height with

reacceleration is  $4 \text{ kpc} < z_h < 12 \text{ kpc}$ . Our new limits should be an improvement on previous estimates because of the more accurate  $Be$  data, our treatment of energy losses, and the inclusion of more realistic astrophysical details (such as, e.g., the gas distribution) in our model.

In case reacceleration is *not* important, the halo size limits are still  $4 \text{ kpc} < z_h < 12 \text{ kpc}$  for the case of no convection, while only the lower limit holds if convection is allowed. The upper limit on the convection velocity gradient is  $dV/dz < 7 \text{ km s}^{-1} \text{ kpc}^{-1}$ , and this value being allowed for large  $z_h$  only.

The gradient of protons derived from gamma rays is smaller than expected for SNR sources, the closest approach to consistency being for  $z_h = 20$  kpc; we therefore adopt a flatter source distribution in order to meet the gamma-ray constraints.

The anisotropy at  $\sim 1$  TeV predicted by our reacceleration models is consistent with observations, while the non-reacceleration model predict a larger value than observed. This reflects the general property of such models (e.g., Seo & Ptuskin 1994). The large-scale propagation is however not significantly constrained by anisotropy measurements at the energies considered in this paper, since local interstellar effects may dominate.

The large  $z_h$  values found here would have very significant implications for gamma rays at high galactic latitudes, giving a larger inverse-Compton intensity than normally considered. Gamma-rays will be addressed in detail in Paper IV.

We are grateful to the referee for useful suggestions. We thank Dr. J. J. Connell for help with the Ulysses  $Be$  data and for providing data prior to publication. We thank Dr. D. Breitschwerdt and Dr. V. Ptuskin for useful discussions.

## APPENDIX

## A. PROPAGATION EQUATION

The propagation equation is written in the form:

$$\frac{\partial \psi}{\partial t} = q(\vec{r}, p) + \vec{\nabla} \cdot (D_{xx} \vec{\nabla} \psi - \vec{V} \psi) + \frac{\partial}{\partial p} p^2 D_{pp} \frac{\partial}{\partial p} \frac{1}{p^2} \psi - \frac{\partial}{\partial p} \left[ \dot{p} \psi - \frac{p}{3} (\vec{\nabla} \cdot \vec{V}) \psi \right] - \frac{1}{\tau_f} \psi - \frac{1}{\tau_r} \psi, \quad (1)$$

where  $\psi = \psi(\vec{r}, p, t)$  is the density per unit of total particle momentum,  $\psi(p) dp = 4\pi p^2 f(\vec{p})$  in terms of phase-space density  $f(\vec{p})$ ,  $q(\vec{r}, p)$  is the source term,  $D_{xx}$  is the spatial diffusion coefficient,  $\vec{V}$  is the convection velocity, reacceleration is described as diffusion in momentum space and is determined by the coefficient  $D_{pp}$ ,  $\dot{p} \equiv dp/dt$  is the momentum loss rate,  $\tau_f$  is the time scale for fragmentation, and  $\tau_r$  is the time scale for the radioactive decay. The details of the numerical scheme is described in Appendix B.

We use particle momentum as the kinematic variable since it greatly facilitates the inclusion of the diffusive reacceleration terms. The injection spectrum of primary nucleons is assumed to be a power law in momentum for the different species,  $dq(p)/dp \propto p^{-\Gamma}$  for the injected *density*<sup>4</sup>, as expected for diffusive shock acceleration (e.g., Blandford & Ostriker 1980); the value of  $\Gamma$  can vary with species. The injection spectrum for <sup>12</sup>C and <sup>16</sup>O was taken as  $dq(p)/dp \propto p^{-2.35}$ , for the case of no reacceleration, and  $p^{-2.25}$  with reacceleration. These values are consistent with Engelmann et al. (1990) who give an injection index  $2.23 \pm 0.05$ . The same indices reproduce the observed proton and <sup>4</sup>He spectra, as was shown in Paper II. For primary electrons, the injection spectrum is adjusted to reproduce direct measurements, gamma-ray and synchrotron data; details are given in the other papers of this series (I, II, IV).

For secondary nucleons, the source term is  $q(\vec{r}, p) = \beta c \psi_p(\vec{r}, p) [\sigma_H^{ps}(p) n_H(\vec{r}) + \sigma_{He}^{ps}(p) n_{He}(\vec{r})]$ , where  $\sigma_H^{ps}(p)$ ,  $\sigma_{He}^{ps}(p)$  are the production cross sections for the secondary from the progenitor on H and He targets,  $\psi_p$  is the progenitor density, and  $n_H$ ,  $n_{He}$  are the interstellar hydrogen and Helium number densities.

To compute  $B/C$  and <sup>10</sup>Be/<sup>9</sup>Be it is sufficient for our purposes to treat only one principal progenitor and compute weighted cross sections based on the observed cosmic-ray abundances, which we took from Lukasiak et al. (1994b). Explicitly, for a principal primary with abundance  $I_p$ , we use for the production cross section  $\bar{\sigma}^{ps} = \sum_i \sigma_i^{is} I_i / I_p$ , where  $\sigma_i^{is}$ ,  $I_i$  are the cross sections and abundances of all species producing the given secondary. For the case of Boron, the Nitrogen progenitor is secondary but only accounts for  $\approx 10\%$  of the total Boron production, so that the approximation of weighted cross sections is sufficient.

For the fragmentation cross sections we use the formula given by Letaw, Silberberg & Tsao (1983). For the secondary production cross sections we use the Webber, Kish & Schrier (1990) and Silberberg & Tsao (1990, see also Garcia-Munoz et al. 1987) parameterizations in the form of code obtained from the Transport Collaboration (Guzik et al. 1997). Comparison of the results from these different versions of the cross sections gives a useful estimate of the uncertainty from this source. For the important  $B/C$  ratio, we take the <sup>12</sup>C, <sup>16</sup>O  $\rightarrow$  <sup>10</sup>B, <sup>10</sup>C, <sup>11</sup>B, <sup>11</sup>C cross sections from the fit to experimental data given by Heinbach & Simon (1995). Since for  $Be$  the values of the cross sections are particularly important we give for reference the values actually used for the abundance-weighted cross sections at 500 MeV/nucleon, including interstellar  $He$ :  $\bar{\sigma}({}^{12}\text{C} \rightarrow {}^9\text{Be}) = 18.2$  mb,  $\bar{\sigma}({}^{12}\text{C} \rightarrow {}^{10}\text{Be}) = 8.6$  mb. For radioactive decay,  $\tau_r = \gamma \tau_{1/2} / \ln 2$ , where  $\tau_{1/2} = 1.6 \times 10^6$  years for <sup>10</sup>Be.

For electrons and positrons the same propagation equation is valid when the appropriate energy loss terms (ionization, bremsstrahlung, inverse Compton, synchrotron) are used. Since this paper is intended to complete the description of the full model, we include the formulae for these loss mechanisms in Appendix C.2. A detailed description of the source function for secondary electrons and positrons was given in Paper II.

## B. NUMERICAL SOLUTION OF PROPAGATION EQUATION

The diffusion, reacceleration, convection and loss terms in eq. (A.1) can all be finite-differenced for each dimension ( $R, z, p$ ) in the form

$$\frac{\partial \psi_i}{\partial t} = \frac{\psi_i^{t+\Delta t} - \psi_i^t}{\Delta t} = \frac{\alpha_1 \psi_{i-1}^{t+\Delta t} - \alpha_2 \psi_i^{t+\Delta t} + \alpha_3 \psi_{i+1}^{t+\Delta t}}{\Delta t} + q_i, \quad (1)$$

where all terms are functions of ( $R, z, p$ ).

In the Crank-Nicholson implicit method (Press et al. 1992) the updating scheme is

$$\psi_i^{t+\Delta t} = \psi_i^t + \alpha_1 \psi_{i-1}^{t+\Delta t} - \alpha_2 \psi_i^{t+\Delta t} + \alpha_3 \psi_{i+1}^{t+\Delta t} + q_i \Delta t. \quad (2)$$

The tridiagonal system of equations,

$$-\alpha_1 \psi_{i-1}^{t+\Delta t} + (1 + \alpha_2) \psi_i^{t+\Delta t} - \alpha_3 \psi_{i+1}^{t+\Delta t} = \psi_i^t + q_i \Delta t, \quad (3)$$

is solved for the  $\psi_i^{t+\Delta t}$  by the standard method (Press et al. 1992). Note that for energy losses we use ‘upwind’ differencing to enhance stability, which is possible since we have only *loss* terms (adiabatic energy *gain* is not included here).

The three spatial boundary conditions

$$\psi(R, z_h, p) = \psi(R, -z_h, p) = \psi(R_h, z, p) = 0 \quad (4)$$

are imposed at each iteration. No boundary conditions are imposed or required at  $R = 0$  or in  $p$ . Grid intervals are typically  $\Delta R = 1$  kpc,  $\Delta z = 0.1$  kpc; for  $p$  a logarithmic scale with ratio typically 1.2 is used. Although the model is symmetric around  $z = 0$  the solution is generated for  $-z_h < z < z_h$  since this is required for the tridiagonal system to be valid.

Since we have a 3-dimensional ( $R, z, p$ ) problem we use ‘operator splitting’ to handle the implicit solution, as follows. We apply the implicit updating scheme alternately for the operator in each dimension in turn, keeping the other two coordinates fixed. To

account for the substeps  $\frac{1}{3}q_i$  and  $\frac{1}{3\tau}$  are used instead of  $q_i$ ,  $1/\tau$ . The coefficients of the Crank-Nicholson scheme we use are given in Table 3.

The method was found to be stable for all  $\alpha$ , and this property can be exploited to advantage by starting with  $\alpha \gg 1$  (see below). The standard alternating direction implicit (ADI) method, in which the full operator is used to update each dimension implicitly in turn, is more accurate but was found to be unstable for  $\alpha > 1$ . This is a disadvantage when treating problems with many timescales, but can be used to generate an accurate solution from an approximation generated by the non-ADI method.

A check for convergence is performed by computing the timescale  $\frac{\psi}{\partial\psi/\partial t}$  from eq. (A.1) and requiring that this be large compared to all diffusive and energy loss timescales. The main problem in applying the method in practice is the wide range of time-scales, especially for the electron case, ranging from  $10^4$  years for energy losses to  $10^9$  years for diffusion around 1 GeV in a large halo. Use of a time step  $\Delta t$  appropriate to the smallest time-scales guarantees a reliable solution, but requires a prohibitively large number of steps to reach the long time-scales. The following technique was found to work well: start with a large  $\Delta t$  appropriate for the longest scales, and iterate until a stable solution is obtained. This solution is then accurate only for cells with  $\alpha \ll 1$ ; for other cells the solution is stable but inaccurate. Then reduce  $\Delta t$  by a factor (0.5 was adopted) and continue the solution. This process is repeated until  $\alpha \ll 1$  for all cells, when the solution is accurate everywhere. It is found that the inaccurate parts of the solution quickly decay as soon as the condition  $\alpha < 1$  is reached for a cell. As soon as all cells satisfy  $\alpha < 1$  the solution is continued with the ADI method to obtain maximum accuracy. A typical run starts with  $\Delta t = 10^9$  years and ends with  $\Delta t = 10^4$  years for nucleons and  $10^2$  years for electrons performing  $\sim 60$  iterations per  $\Delta t$ . In this way it is possible to obtain reliable solutions in a reasonable computer resources, although the CPU required is still considerable. All results are output as FITS datasets for subsequent analysis.

More details, including the software and datasets, can be found on the World Wide Web (address available from the authors).

### B.1. DIFFUSION IN R

As an example, the coefficients for the radial diffusion term are derived here.

$$\frac{1}{R} \frac{\partial}{\partial R} \left( R D_{xx} \frac{\partial \psi}{\partial R} \right) = \frac{2}{R_i} \frac{D_{xx}}{R_{i+1} - R_{i-1}} \left\{ R_{i+1} \frac{\psi_{i+1} - \psi_i}{R_{i+1} - R_i} - R_{i-1} \frac{\psi_i - \psi_{i-1}}{R_i - R_{i-1}} \right\}. \quad (5)$$

Setting  $R_{i+1} - R_i = R_i - R_{i-1} = \Delta R$ , one can obtain the following expressions in terms of our standard form (eq. [A.1])

$$\frac{\alpha_1}{\Delta t} = D_{xx} \frac{2R_i - \Delta R}{2R_i(\Delta R)^2}, \quad \frac{\alpha_2}{\Delta t} = D_{xx} \frac{2R_i}{R_i(\Delta R)^2}, \quad \frac{\alpha_3}{\Delta t} = D_{xx} \frac{2R_i + \Delta R}{2R_i(\Delta R)^2}. \quad (6)$$

<sup>4</sup> This corresponds to an injected flux  $dF(p)/dp \propto \beta p^{-\Gamma}$  or  $dF(E_k)/dE_k \propto p^{-\Gamma}$ , a form often used (e.g., Engelmann et al. 1990). Since observations are usually quoted as a flux with kinetic energy per nucleon as the kinematic variable a conversion is made before comparison with data:  $dF(E_k)/dE_k = \frac{c}{4\pi} \beta \psi(dp/dE_k) = \frac{c}{4\pi} A \psi$  since  $dp/dE_k = A/\beta$ , where  $A$  is the mass number,  $E_k$  is the kinetic energy per nucleon,  $\beta = v/c$ .

TABLE 3  
COEFFICIENTS FOR THE CRANK-NICHOLSON METHOD.

Process	Coordinate	$\alpha_1/\Delta t$	$\alpha_2/\Delta t$	$\alpha_3/\Delta t$
Diffusion	$R$	$D_{xx} \frac{2R_i - \Delta R}{2R_i(\Delta R)^2}$	$D_{xx} \frac{2R_i}{R_i(\Delta R)^2}$	$D_{xx} \frac{2R_i + \Delta R}{2R_i(\Delta R)^2}$
	$z$	$D_{xx}/(\Delta z)^2$	$2D_{xx}/(\Delta z)^2$	$D_{xx}/(\Delta z)^2$
Convection <sup>a</sup>	$z > 0$ ( $V > 0$ )	$V(z_{i-1})/\Delta z$	$V(z_i)/\Delta z$	0
	$z < 0$ ( $V < 0$ )	0	$-V(z_i)/\Delta z$	$-V(z_{i+1})/\Delta z$
	$p$ ( $dV/dz > 0$ )	0	$-\frac{1}{3} p_i \frac{dV}{dz} / P_{i-1}^i$	$-\frac{1}{3} p_{i+1} \frac{dV}{dz} / P_i^{i+1}$
Diffusive reacceleration <sup>a</sup>	$p$	$\frac{2D_{pp,i-1}}{P_{i-1}^{i+1}} \left( \frac{1}{P_{i-1}^i} + \frac{2}{P_{i-1}} \right)$	$\frac{2}{P_{i-1}^{i+1}} \left( \frac{D_{pp,i+1}}{P_i^{i+1}} + \frac{D_{pp,i-1}}{P_{i-1}^i} \right)$	$\frac{2D_{pp,i+1}}{P_{i-1}^{i+1}} \left( \frac{1}{P_i^{i+1}} - \frac{2}{P_{i+1}} \right)$
Energy loss <sup>a</sup>	$p$	0	$\dot{p}_i / P_i^{i+1}$	$\dot{p}_{i+1} / P_i^{i+1}$
Fragmentation	$R, z, p$	0	$1/3\tau_f$	0
Radioactive decay	$R, z, p$	0	$1/3\tau_r$	0

<sup>a</sup>  $P_j^i \equiv p_i - p_j$

### B.2. DIFFUSIVE REACCELERATION

In terms of 3-D momentum phase-space density  $f(\vec{p})$  the diffusive reacceleration equation is

$$\frac{\partial f(\vec{p})}{\partial t} = \vec{\nabla}_p \cdot [D_{pp} \vec{\nabla}_p f(\vec{p})] = \frac{1}{p^2} \frac{\partial}{\partial p} \left[ p^2 D_{pp} \frac{\partial f(p)}{\partial p} \right]. \quad (7)$$

The distribution is assumed isotropic so  $f(\vec{p}) = f(p)$  where  $p = |\vec{p}|$ . First we rewrite the equation in terms of  $\psi(p) = 4\pi p^2 f(p)$  instead of  $f(p)$  and expand the inner differential:

$$\frac{\partial \psi}{\partial t} = \frac{\partial}{\partial p} \left[ p^2 D_{pp} \frac{\partial \psi}{\partial p} \right] = \frac{\partial}{\partial p} D_{pp} \left[ \frac{\partial \psi}{\partial p} - \frac{2\psi}{p} \right]. \quad (8)$$

The differencing scheme is then

$$\frac{2}{p_{i+1} - p_{i-1}} \left[ D_{pp,i+1} \left( \frac{\psi_{i+1} - \psi_i}{p_{i+1} - p_i} - \frac{2\psi_{i+1}}{p_{i+1}} \right) - D_{pp,i-1} \left( \frac{\psi_i - \psi_{i-1}}{p_i - p_{i-1}} - \frac{2\psi_{i-1}}{p_{i-1}} \right) \right]. \quad (9)$$

In terms of our standard form (eq. [A.1]) the coefficients for reacceleration are

$$\begin{aligned} \frac{\alpha_1}{\Delta t} &= \frac{2D_{pp,i-1}}{p_{i+1} - p_{i-1}} \left( \frac{1}{p_i - p_{i-1}} + \frac{2}{p_{i-1}} \right), \\ \frac{\alpha_2}{\Delta t} &= \frac{2}{p_{i+1} - p_{i-1}} \left( \frac{D_{pp,i+1}}{p_{i+1} - p_i} + \frac{D_{pp,i-1}}{p_i - p_{i-1}} \right), \\ \frac{\alpha_3}{\Delta t} &= \frac{2D_{pp,i+1}}{p_{i+1} - p_{i-1}} \left( \frac{1}{p_{i+1} - p_i} - \frac{2}{p_{i+1}} \right). \end{aligned} \quad (10)$$

### C. ENERGY LOSSES

For nucleon propagation in the ISM the losses are mainly due to ionization, Coulomb scattering, fragmentation, and radioactive decay. For electrons the important processes are ionization, Coulomb scattering, bremsstrahlung in the neutral and ionized medium, as well as Compton and synchrotron losses. Although all these processes are well-known the formulae for the different cases are rather scattered throughout the literature and hence for completeness we summarize the formulae used below.

Figure 13 illustrates the energy loss time scales,  $E(dE/dt)^{-1}$ , for electrons and nucleons in pure hydrogen. The losses are shown for equal neutral and ionized gas number densities  $n_H = n_{HI} = 0.01 \text{ cm}^{-3}$ , and equal energy densities of photons and the magnetic field  $U = U_B = 1 \text{ eV cm}^{-3}$  (in the Thomson limit). These gas and energy densities are chosen to characterize the average values seen by cosmic-rays during propagation.

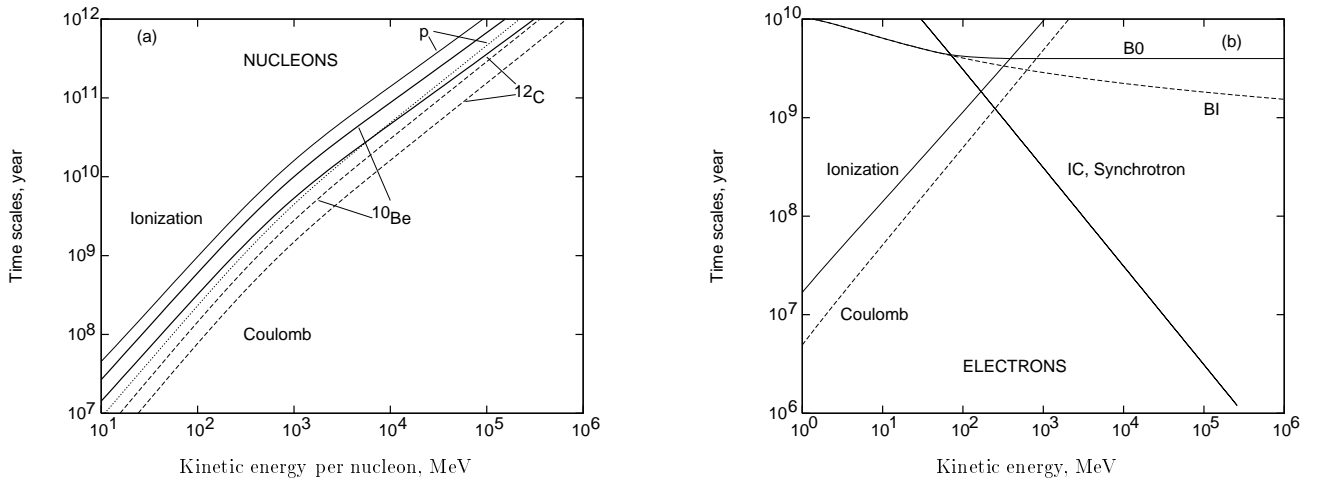


FIG. 13.— Energy loss time-scales of (a) nucleons and (b) electrons in neutral and ionized hydrogen. The curves are computed for gas densities  $n_H = n_{HI} = 0.01 \text{ cm}^{-3}$ , and equal energy densities of photons and magnetic field  $U = U_B = 1 \text{ eV cm}^{-3}$  (in the Thomson limit). In panel (a) solid lines correspond to ionization losses and dashed lines to Coulomb losses (the dotted line is that for protons).

#### C.1. NUCLEON ENERGY LOSSES

The Coulomb collisions in a completely ionized plasma are dominated by scattering off the thermal electrons. The corresponding energy losses are given by (Mannheim & Schlickeiser 1994, their eqs. [4.16],[4.22])

$$\left( \frac{dE}{dt} \right)_{\text{Coul}} \approx -4\pi r_e^2 c m_e c^2 Z^2 n_e \ln \Lambda \frac{\beta^2}{x_m^3 + \beta^3}, \quad (1)$$

where  $r_e$  is the classical electron radius,  $m_e$  is the electron rest mass,  $c$  is the velocity of light,  $Z$  is the *projectile* nucleon charge,  $\beta = v/c$  is the nucleon speed,  $n_e$  is the electron number density in plasma,  $x_m \equiv (3\sqrt{\pi}/4)^{1/3} \times \sqrt{2kT_e/m_e c^2}$ , and  $T_e$  is the electron temperature. The Coulomb logarithm in the cold plasma limit is given by (e.g., Dermer 1985)

$$\ln \Lambda \approx \frac{1}{2} \ln \left( \frac{m_e^2 c^4}{\pi r_e \hbar^2 c^2 n_e} \cdot \frac{M \gamma^2 \beta^4}{M + 2\gamma m_e} \right), \quad (2)$$

where  $\hbar$  is the Planck constant,  $M$  is the nucleon mass, and  $\gamma$  is the nucleon Lorentz factor. For the appropriate number density,  $n_e \sim 10^{-1} - 10^{-3} \text{ cm}^{-3}$ , and total energy  $E \sim 10^3 - 10^4 \text{ MeV}$ , the typical value of the Coulomb logarithm  $\ln \Lambda$  lies within interval  $\sim 40 - 50$ , instead of usually adopted value 20.

For the ionization losses we use a general formula (Mannheim & Schlickeiser 1994, their eq. [4.24])

$$\left( \frac{dE}{dt} \right)_I (\beta \geq \beta_0) = -2\pi r_e^2 c m_e c^2 Z^2 \frac{1}{\beta} \sum_{s=H,He} n_s [B_s + B'(\alpha_f Z/\beta)], \quad (3)$$

where  $\alpha_f$  is the fine structure constant,  $n_s$  is the number density of the corresponding species in the ISM,  $\beta_0 = 1.4e^2/\hbar c = 0.01$  is the characteristic velocity determined by the orbital velocity of the electrons in hydrogen, and

$$B_s = \left[ \ln \left( \frac{2m_e c^2 \beta^2 \gamma^2 Q_{\max}}{\tilde{I}_s^2} \right) - 2\beta^2 - \frac{2C_s}{z_s} - \delta_s \right], \quad (4)$$

where  $\gamma$  is the Lorentz factor of the ion. The largest possible energy transfer from the incident particle to the atomic electron is defined by kinematics<sup>5</sup>

$$Q_{\max} \approx \frac{2m_e c^2 \beta^2 \gamma^2}{1 + [2\gamma m_e/M]}, \quad (5)$$

where  $M \gg m_e$  is the nucleon mass, and  $\tilde{I}_s$  denotes the geometric mean of all ionization and excitation potentials of the atom. Mannheim & Schlickeiser (1994) give the values  $\tilde{I}_H = 19 \text{ eV}$  and  $\tilde{I}_{He} = 44 \text{ eV}$ . The shell-correction term  $C_s/z_s$ , the density correction term  $\delta_s$ , and the  $B'$  correction term (for large  $Z$  or small  $\beta$ ) in eqs. (C.3),(C.4), can be neglected for our purposes.

Fragmentation and radioactive decay are addressed in Appendix A.

### C.2. ELECTRON ENERGY LOSSES

Ionization losses in the neutral hydrogen and helium are given by the Bethe-Bloch formula (Ginzburg 1979, p.360)

$$\left( \frac{dE}{dt} \right)_I = -2\pi r_e^2 c m_e c^2 \frac{1}{\beta} \sum_{s=H,He} Z_s n_s \left[ \ln \left\{ \frac{(\gamma-1)\beta^2 E^2}{2I_s^2} \right\} + \frac{1}{8} \right], \quad (6)$$

where  $Z_s$  is the nucleus charge,  $n_s$  is the gas number density,  $I_s$  is the ionization potential (we use  $I_H = 13.6 \text{ eV}$ ,  $I_{He} = 24.6 \text{ eV}$ , though the exact numbers are not very important),  $E$  is the total electron energy,  $\gamma$  and  $\beta = v/c$  are the electron Lorentz factor and speed, correspondingly.

The Coulomb energy losses in the fully ionized medium, in the cold plasma limit, are described by (Ginzburg 1979, p.361)

$$\left( \frac{dE}{dt} \right)_{\text{Coul}} = -2\pi r_e^2 c m_e c^2 Z n \frac{1}{\beta} \left[ \ln \left( \frac{Em_e c^2}{4\pi r_e \hbar^2 c^2 n Z} \right) - \frac{3}{4} \right], \quad (7)$$

where  $Zn \equiv n_e$  is the electron number density. For an accurate treatment of the electron energy losses in the plasma of an arbitrary temperature see, e.g., Dermer & Liang (1989) and Moskalenko & Jourdain (1997).

The energy losses due to  $ep$ -bremsstrahlung in the cold plasma are given by the expression (von Stickforth 1961)

$$\left( \frac{dE}{dt} \right)_{ep} = -\frac{2}{3} \alpha_f r_e^2 c m_e c^2 Z^2 n \begin{cases} 8\gamma\beta [1 - 0.25(\gamma-1) + 0.44935(\gamma-1)^2 - 0.16577(\gamma-1)^3], & \gamma \leq 2; \\ \beta^{-1} [6\gamma \ln(2\gamma) - 2\gamma - 0.2900], & \gamma \geq 2. \end{cases} \quad (8)$$

For the  $ee$ -bremsstrahlung one can obtain (Haug 1975, Moskalenko & Jourdain 1997)

$$\left( \frac{dE}{dt} \right)_{ee} = -\frac{1}{2} \alpha_f r_e^2 c m_e c^2 Z n \beta \gamma^* Q_{\text{cm}}(\gamma^*), \quad (9)$$

where

$$Q_{\text{cm}}(\gamma^*) = 8 \frac{p^{*2}}{\gamma^*} \left[ 1 - \frac{4p^*}{3\gamma^*} + \frac{2}{3} \left( 2 + \frac{p^{*2}}{\gamma^{*2}} \right) \ln(p^* + \gamma^*) \right],$$

$$\gamma^* = \sqrt{(\gamma+1)/2},$$

$$p^* = \sqrt{(\gamma-1)/2},$$

<sup>5</sup>note that there was a typing mistake in the denominator of the expression given by Mannheim & Schlickeiser (1994), which is corrected in our formula.

and the asterisk denotes center-of-mass variables. The total bremsstrahlung losses in the ionized gas is the sum  $(dE/dt)_{\text{BI}} = (dE/dt)_{ep} + (dE/dt)_{ee}$ . A good approximation gives the expression (Ginzburg 1979, p.408)

$$\left(\frac{dE}{dt}\right)_{\text{BI}} = -4\alpha_f r_e^2 c m_e c^2 Z(Z+1)nE \left[ \ln(2\gamma) - \frac{1}{3} \right]. \quad (10)$$

Bremsstrahlung energy losses in neutral gas can be obtained by integration over the bremsstrahlung luminosity (Koch & Motz 1959, see also Paper IV)

$$\left(\frac{dE}{dt}\right)_{\text{B0}} = -c\beta \sum_{s=H,He} n_s \int dk k \frac{d\sigma_s}{dk}. \quad (11)$$

A suitable approximation (max 10% error near  $E \sim 70$  MeV) for eq. (C.11) gives the combination (cf. eq. [C.10])

$$\left(\frac{dE}{dt}\right)_{\text{B0}} = \begin{cases} -4\alpha_f r_e^2 c m_e c^2 E \left[ \ln(2\gamma) - \frac{1}{3} \right] \sum_{s=H,He} n_s Z_s (Z_s + 1), & \gamma \lesssim 100; \\ -cE \sum_{s=H,He} \frac{n_s M_s}{T_s}, & \gamma \gtrsim 800, \end{cases} \quad (12)$$

(see Ginzburg 1979, p.386, 409), with a linear connection in between. Here  $M_s$  is the atomic mass, and  $T_s$  is the radiation length ( $T_H \simeq 62.8$  g/cm<sup>2</sup>,  $T_{He} \simeq 93.1$  g/cm<sup>2</sup>).

The Compton energy losses are calculated using the Klein-Nishina cross section (Jones 1965, Moskalenko & Jourdain 1997)

$$\frac{dE}{dt} = \frac{\pi r_e^2 m_e c^2 c}{2\gamma^2 \beta} \int_0^\infty d\omega f_\gamma(\omega) [S(\gamma, \omega, k^+) - S(\gamma, \omega, k^-)], \quad (13)$$

where the background photon distribution,  $f_\gamma(\omega)$ , is normalized on the photon number density as  $n_\gamma = \int d\omega \omega^2 f_\gamma(\omega)$ ,  $\omega$  is the energy of the background photon taken in the electron-rest-mass units,  $k^\pm = \omega\gamma(1 \pm \beta)$ ,

$$S(\gamma, \omega, k) = \omega \left\{ \left( k + \frac{31}{6} + \frac{5}{k} + \frac{3}{2k^2} \right) \ln(2k+1) - \frac{11}{6}k - \frac{3}{k} + \frac{1}{12(2k+1)} + \frac{1}{12(2k+1)^2} + Li_2(-2k) \right\} \\ - \gamma \left\{ \left( k + 6 + \frac{3}{k} \right) \ln(2k+1) - \frac{11}{6}k + \frac{1}{4(2k+1)} - \frac{1}{12(2k+1)^2} + 2Li_2(-2k) \right\}, \quad (14)$$

and  $Li_2$  is the dilogarithm

$$Li_2(-2k) = - \int_0^{-2k} dx \frac{1}{x} \ln(1-x) \\ = \begin{cases} \sum_{i=1}^\infty (-2k)^i / i^2, & k \leq 0.2; \\ -1.6449341 + \frac{1}{2} \ln^2(2k+1) - \ln(2k+1) \ln(2k) + \sum_{i=1}^\infty i^{-2} (2k+1)^{-i}, & k \geq 0.2. \end{cases} \quad (15)$$

The synchrotron energy losses are given by

$$\left(\frac{dE}{dt}\right)_s = -\frac{32}{9} \pi r_e^2 c U_B \gamma^2 \beta^2, \quad (16)$$

where  $U_B = \frac{H^2}{8\pi}$  is the energy density of the random magnetic field.

## REFERENCES

- Barwick, S. W., et al. 1997, *ApJ*, 482, L191
- Barwick, S. W., et al. 1998, *ApJ*, 498, 779
- Berezinskii, V. S., et al. 1990, *Astrophysics of Cosmic Rays* (Amsterdam: North Holland)
- Blandford, R. D., & Ostriker, J. P. 1980, *ApJ*, 237, 793
- Bloemen, H., Dogiel, V. A., Dorman, V. I., & Ptuskin, V. S. 1993, *A&A*, 267, 372
- Bronfman, L., et al. 1988, *ApJ*, 324, 248
- Case, G., & Bhattacharya, D. 1996, *A&AS*, 120C, 437
- Connell, J. J. 1998, *ApJ*, 501, L59
- Cordes, J. M., et al. 1991, *Nature*, 354, 121
- Cox, P., Krügel, E., & Mezger, P. G. 1986, *A&A*, 155, 380
- Dermer, C. D. 1985, *ApJ*, 295, 28
- Dermer, C. D., & Liang, E. P. 1989, *ApJ*, 339, 512
- DuVernois, M. A., Simpson, J. A., & Thayer, M. R. 1996, *A&A*, 316, 555
- Engelmann, J. J., et al. 1985, *A&A*, 148, 12
- Engelmann, J. J., et al. 1990, *A&A*, 233, 96
- Ferrando, P., et al. 1996, *A&A*, 316, 528
- Freedman, I., Kearsley, S., & Osborne, J. L., Giler, M. 1980, *A&A*, 82, 110
- Garcia-Munoz, M., et al. 1987, *ApJS*, 64, 269
- Ginzburg, V. L. 1979, *Theoretical Physics and Astrophysics* (Oxford: Pergamon Press)
- Ginzburg, V. L., Khazan, Ya. M., & Ptuskin, V. S. 1980, *Ap&SS*, 68, 295
- Gleeson, L. J., & Axford, W. I. 1968, *ApJ*, 154, 1011
- Gordon, M. A., & Burton, W. B. 1976, *ApJ*, 208, 346
- Green, D. A. 1991, *PASP*, 103, 209
- Grevesse, N., Noels, A. & Sauval A. J. 1996, in *ASP Conf. Ser 99, Cosmic Abundances*, ed. S. S. Holt & G. Sonneborn (San Francisco: ASP), 117
- Guzik, T. G., et al. 1997, *Proc. 25th Int. Cosmic Ray Conference*, 4, 317
- Haug, E. 1975, *Z. Naturforsch.*, 30a, 1546
- Heiles, C. 1996, *ApJ*, 462, 316
- Heinbach, U., & Simon, M. 1995, *ApJ*, 441, 209
- Hernandez, F. P., & Christensen-Dalsgaard, J. 1994, *MNRAS*, 269, 475
- Hunter, S. D., et al. 1997, *ApJ*, 481, 205
- Johnston, S. 1994, *MNRAS*, 268, 595
- Jokipii, J. R. 1976, *ApJ*, 208, 900
- Jones, F. C. 1965, *Phys. Rev.*, 137, B1306
- Jones, F. C. 1979, *ApJ*, 229, 747
- Koch, H. W., & Motz, J. W. 1959, *Rev. Mod. Phys.*, 31, 920
- Lerche, I., & Schlickeiser, R. 1982, *A&A*, 107, 148
- Letaw, J. R., Silberberg, R., & Tsao, C. H. 1983, *ApJS*, 51, 271
- Letaw, J. R., Silberberg, R., & Tsao, C. H. 1993, *ApJ*, 414, 601
- Lukasiak, A., Ferrando, P., McDonald F. B., & Webber, W. R. 1994a, *ApJ*, 423, 426
- Lukasiak, A., Ferrando, P., McDonald F. B., & Webber, W. R. 1994b, *ApJ*, 426, 366
- Mannheim, K., & Schlickeiser, R. 1994, *A&A*, 286, 983
- Meyer, J.-P., Drury, L. O'C., & Ellison D. C. 1997, *ApJ*, 487, 182
- Moskalenko, I. V., & Jourdain, E. 1997, *A&A*, 325, 401
- Moskalenko, I. V., & Strong, A. W. 1998a, *ApJ*, 493, 694 (Paper II)
- Moskalenko, I. V., & Strong, A. W. 1998b, in preparation (Paper IV)
- Owens, A. J., & Jokipii, J. R. 1977a, *ApJ*, 215, 677
- Owens, A. J., & Jokipii, J. R. 1977b, *ApJ*, 215, 685
- Phillipps, S., et al. 1981, *A&A*, 103, 405
- Press, W. H. et al. 1992, *Numerical Recipes in FORTRAN*, 2nd Edition (Cambridge: Cambridge University Press)
- Porter, T. A., & Protheroe R. J. 1997, *J. Phys. G.: Nucl. Part. Phys.*, 23, 1765
- Ptuskin, V. S., Völk, H. J., Zirakashvili, V. N., & Breitschwerdt, D. 1997, *A&A*, 321, 434
- Reynolds, R. J. 1989, *ApJ*, 339, L29
- Seo, E. S., et al. 1991, *ApJ*, 378, 763
- Seo, E. S., & Ptuskin, V. S. 1994, *ApJ*, 431, 705
- Silberberg, R., & Tsao, C. H. 1990, *Phys. Rep.*, 191, 351
- Simon, M., & Heinbach, U. 1996, *ApJ*, 456, 519
- Simpson, J. A., & Garcia-Munoz, M. 1988, *Spa. Sci. Rev.*, 46, 205
- von Stickforth, J. 1961, *Z. Physik*, 164, 1
- Strong, A. W. 1996, *Spa. Sci. Rev.*, 76, 205
- Strong, A. W., & Mattox, J. R. 1996, *A&A*, 308, L21
- Strong, A. W., & Moskalenko, I. V. 1997, in *AIP Conf. Proc. 410, Fourth Compton Symposium*, ed. C. D. Dermer, M. S. Strickman, & J. D. Kurfess (New York: AIP), p.1162 (Paper I)
- Strong, A. W., & Youssefi, G. 1995, *Proc. 24th Int. Cosmic Ray Conf. (Roma)*, 3, 48
- Strong, A. W., Moskalenko, I. V., & Schönfelder, V. 1997, *25th Int. Cosmic Ray Conf. (Durban)*, 4, 257
- Strong, A. W., et al. 1996, *A&AS*, 120C, 381
- Taylor, J. H., Manchester, R. N., & Lyne, A. G. 1993, *ApJS*, 88, 529
- Webber, W. R. 1997, *Spa. Sci. Rev.* 81, 107
- Webber, W. R., Kish, J. C., & Schrier, D. A. 1990, *Phys. Rev. C*, 41, 566
- Webber, W. R., Lee, M. A., & Gupta, M. 1992, *ApJ*, 390, 96
- Webber, W. R., Lukasiak, A., McDonald, F. B., Ferrando, P. 1996, *ApJ*, 457, 435
- Zirakashvili, V. N., Breitschwerdt, D., Ptuskin, V. S., & Völk, H. J. 1996, *A&A*, 311, 113